Electron Interferometry at a Heterojunction Interface

J. A. Kubby, Y. R. Wang, and W. J. Greene
Xerox Webster Research Center, 800 Phillips Road, Webster, New York 14580
(Received 7 June 1990)

We have used the tunneling microscope to excite electron standing waves over clean and adsorbate-covered surfaces. For smooth, continuous overlayers we observe a resonance in the conductivity spectra that is absent on the clean surface, over film defects, and over film areas that are rough on a length scale of the electron's de Broglie wavelength. By making reasonable assumptions of the adlayer thickness and interface scattering strength, the resonance can be modeled by a quantum-size effect in electron transmission through the adlayer.

PACS numbers: 61.16.Di, 68.35.Bs, 73.20.At

The tunneling microscope has proven to be a powerful technique for locally probing the atomic structure of clean semiconducting surfaces on a length scale of a few angstroms.[1] As interest shifts from the study of clean to adsorbate-covered surfaces, it would be useful to extend the capabilities of the microscope to include localized studies of buried heterointerfaces.[2] We have utilized electron standing waves excited by the tunneling microscope[3-5] for the first atomic resolution structural study of a buried heterointerface. *We believe that these data provide the first causal connection between geometric structure, the Sn/Si(111) interface, and how it manifests itself in the measured density of states.* The detection of standing-wave formation between a surface and buried interface has been previously reported for thin-film tunnel diodes,[6] and in retarding-field measurements.[7,8] In the following we use the tunneling microscope to investigate these quantum-size effects[6-8] (QSE) in tunneling through thin-film overlayers. This technique has the advantage of being localized on an atomic length scale, as well as rendering a real space image of the area that is being probed.

The samples used in this study were cut from an arsenic-doped, 0.005-Ω cm Si(111) wafer. Approximately $\frac{1}{3}$ ML (monolayer) of tin was deposited onto the room-temperature substrate from a tungsten-filament source at a deposition rate of 1 ML/min. After deposition, the sample was annealed at 550 °C for 2 min to generate the $\sqrt{3}$ and $2\sqrt{3}$ reconstructions, and at 800 °C for 2 min to generate the $\sqrt{3}$ mosaic surface. The operation of the microscope to obtain conductivity maps has been described previously.[5]

Figure 1 shows topographic images of the $\sqrt{3}$, $2\sqrt{3}$, and $\sqrt{3}$ mosaic regions we have observed on this surface. The $2\sqrt{3}$ and $\sqrt{3}$ reconstructions shown in Fig. 1(a) have been observed previously by LEED,[9] reflection high-energy electron diffraction,[10] and scanning tunneling microscopy (STM).[11] The STM results[11] indicate that the $\sqrt{3}$ adatoms lie in threefold-coordinated sites above a second-layer Si atom, in the T_4 adsorption site. The different areas shown in this figure were characterized by exciting electron standing waves over the respective areas, with the resulting conductivity spectra shown in Fig. 2.

In Fig. 2(a), the standing-wave spectrum was collected over the $2\sqrt{3}$ area to the left in Fig. 1(a). The standing-wave spectrum shown in Fig. 2(b) was collected over the

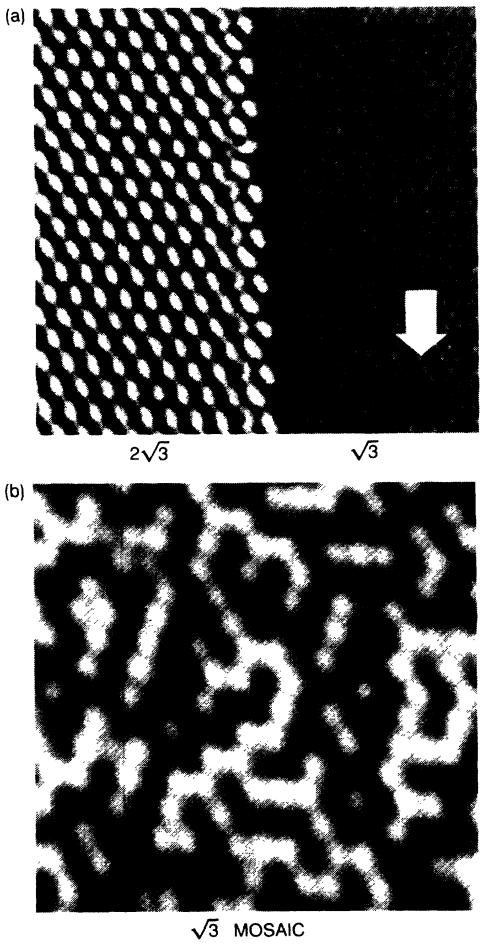

FIG. 1. Tunneling topographs of areas used for standing-wave excitation. (a) 250×250-Å area containing $2\sqrt{3}$ reconstruction on the left and $\sqrt{3}$ reconstruction on the right. The gray scale is keyed to curvature to emphasize local height. (b) 100×100-Å $\sqrt{3}$ mosaic region. The gray scale is keyed to apparent height with a total range of 1.5 Å. Both images were collected with a tip bias of −1.5 V, tunneling from tip to sample at a demanded current of 1 nA.

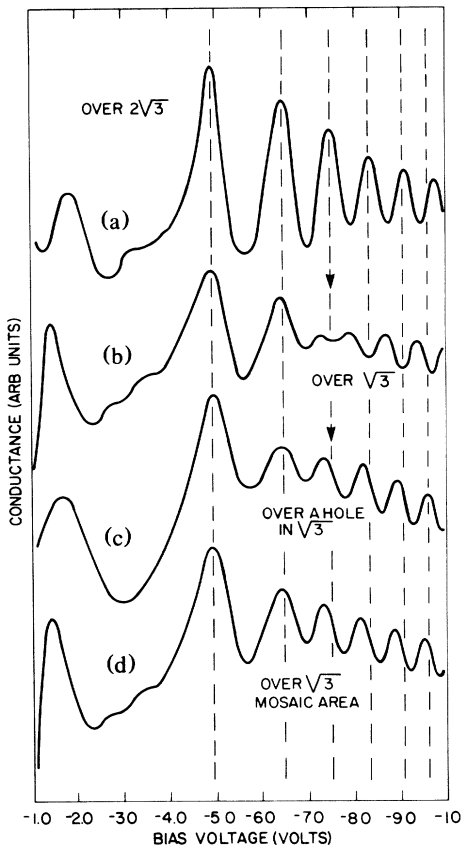

FIG. 2. Conductance vs applied bias spectra for various areas on the Sn/Si(111) surface: (a) over $2\sqrt{3}$ region, (b) over $\sqrt{3}$ region, (c) over a hole in the $\sqrt{3}$ region, and (d) over $\sqrt{3}$ mosaic region. The demanded tunneling current was 1 nA.

$\sqrt{3}$ area to the right. Several spectra were collected alternately over each of these areas with reproducible spectra indicating that any differences in the spectra are associated with differences in the sample rather than artifacts in the tip electronic structure.

Below -5-V bias both standing-wave spectra exhibit a maximum near -1.5 eV, with the maximum shifted upwards by 0.2 eV on the $2\sqrt{3}$ surface and down by 0.2 eV on the $\sqrt{3}$ surface. This feature is similar in energy to an adatom T_4 backbonding state seen on Si(111)-7×7 with the tunneling microscope[5] and is assumed to be associated with a similar Sn-induced adatom state.

Above -5-V bias both standing-wave spectra exhibit conductivity oscillations at biases corresponding to the formation of electron standing waves between the tip and the sample;[4] however, over the $\sqrt{3}$ area there is additional structure at -7.5 eV that is absent over the $2\sqrt{3}$ area. This feature has been marked by an arrow in Fig. 2(b). This feature has been reproduced with a number of surface preparations and with a number of tips. While the number of standing-wave oscillations between -5 and -10 eV changes with the macroscopic sharpness of the tip or the demanded tunneling current, the energy position of this feature does not.

In addition to the resonance observed at -7.5 eV over the $\sqrt{3}$ area, an effect due to the resonance can be seen on the higher-order standing-wave maxima. Below the resonance the first two standing-wave maxima line up in the spectra taken over the $2\sqrt{3}$ and $\sqrt{3}$ areas shown in Figs. 2(a) and 2(b). However, beyond the -7.5-eV resonance there is a 180° phase shift between the peaks in the two standing-wave spectra. It appears that the presence of the resonance has displaced the higher-order standing-wave peaks to higher biases. The dashed lines in Fig. 2 have been drawn in to guide the eye in seeing this shift.

If a standing-wave spectrum is taken over a hole in the $\sqrt{3}$ area, marked by an arrow in Fig. 1(a), the -7.5-eV feature is absent, as shown in the spectrum of Fig. 2(c), although a broadened peak below -5 eV is still seen. If a spectrum is collected over the $\sqrt{3}$ mosaic region shown in Fig. 1(b), the -7.5-eV feature is also absent, as shown in Fig. 2(d), *yet the density of states below -5 eV is identical to the spectrum of Fig. 2(b).* Thus the peak at -7.5 eV is absent over "rough" areas such as $2\sqrt{3}$, a $\sqrt{3}$ defect, or $\sqrt{3}$ mosaic, while the lower-lying structure remains. In addition to the lack of a -7.5-eV resonance over the rough areas, the phase shifts in the higher-order standing-wave peaks in the spectra shown in Figs. 2(c) and 2(d) are also reduced.

To investigate the sensitivity of the -7.5-eV resonance to film inhomogeneities, we have collected conductivity maps[5] over the defective $\sqrt{3}$ area shown in Fig. 3(a). The conductivity maps in Figs. 3(b)–3(e) were collected one after the other as the bias was incremented from -7 to -7.75 eV, through the resonance at -7.5 eV. Although the tip is some 16 Å away from the surface at this bias, the ballistic electron field-emission current is relatively focused[12] and thus atomic resolution is obtained. A small amount of drift occurs between each frame, but characteristic features can be followed from frame to frame; the cluster of five defects in the upper left-hand corner of topograph 3(a) has drifted down to the lower right-hand corner of the conductivity map in 3(e). The defects with bright halos in the topograph shown in 3(a) appear as low-conductivity (dark) features in the conductance map 3(b) at -7 eV, whereas the defects without halos in the topograph appear as high-conductivity (light) features at this bias. As the bias is swept through the resonance condition, a 180° phase shift in the defect conductivity (dark to bright, bright to dark) can be seen between images 3(b) and 3(d), and also between images 3(c) and 3(e). A similar phase shift was observed in conductivity maps of the Si(111)-7×7 stacking fault as a function of bias.[13] From this sequence of images it is clear that the continuous film is an equal conductance surface through the resonance, with areas of film defects being off resonance and thus rendering localized contrast in the conductivity map.

We have modeled electron transport through the ad-

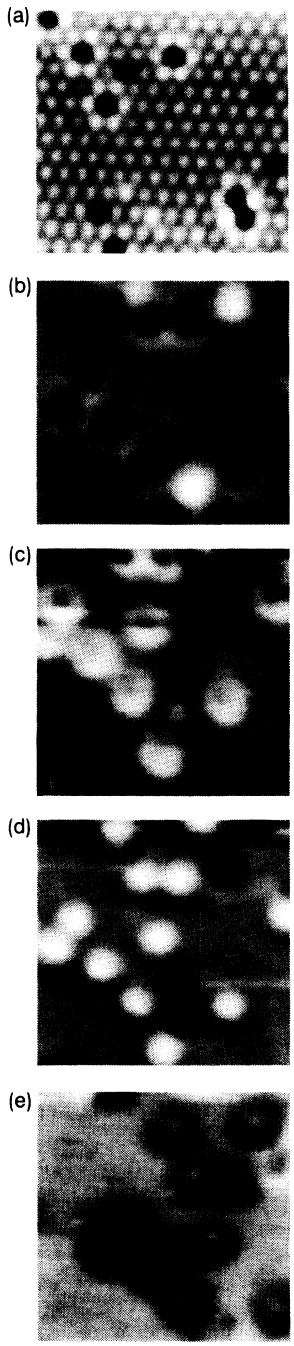

FIG. 3. Conductivity maps of the defective $\sqrt{3}$ area. (a) 100×100-Å topograph at a tip bias of +1.3 V and a demanded tunneling current of 1 nA; (b) conductivity map at −7.0 V, (c) at −7.25 V, (d) at −7.50 V, and (e) at −7.75 V.

layer using the potential-energy diagram shown in Fig. 4. In this model[13] we have placed the interface scattering potential V_i at a depth of 1.44 Å to place the calculated resonance at −7.5 eV, as found in the experimental spectra. This depth is in reasonable agreement with the 1.5-Å adatom height determined from the $\sqrt{3}$ mosaic image

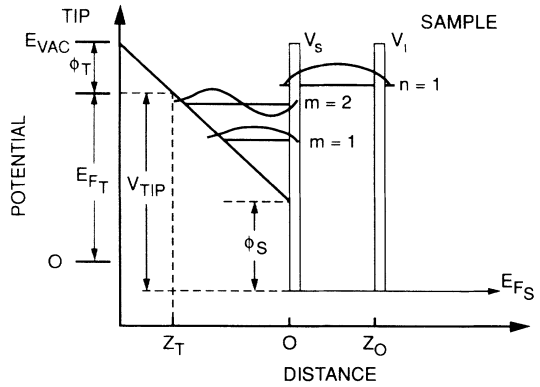

FIG. 4. Potential-energy diagram of the tip-sample junction used in the calculations. In this figure Φ_T, E_{F_T} and Φ_S, E_{F_S} are the work functions and Fermi energies of the tip and sample, respectively. V_s and V_i are the δ-function strengths of the surface (at $Z=0$) and the buried interface (at $Z=Z_0$) scattering potentials, respectively. V_T is the applied (negative) tip bias. The first two electron standing-wave states excited between the classical turning point (at $Z=Z_T$) and the sample surface have been labeled $m=1,2$ and the first electron standing-wave state excited between the surface and buried interface has been labeled $n=1$.

in Fig. 1(b), although a height measurement from a tunneling topograph will reflect electronic as well as geometric structure. This adsorption height is also similar to the equilibrium position calculated for silicon adatoms in T_4 sites.[14]

Figure 5 shows our calculated differential conductivity as a function of the applied gap bias for a constant demanded tunneling current of 1 nA. An oscillatory behavior of the conductivity beyond a gap bias of −5 eV is obtained for $V_s=V_i=0$ in Fig. 5(a) as has been previously reported[4,5] in association with electron standing-wave formation. Here each successive oscillation in dI/dV incorporates an additional standing wave in the gap, labeled as $m=1,2$ in Fig. 4. This basic feature of the conductivity does not change with the inclusion of a surface δ-function potential, as shown by the standing-wave peaks labeled $m=1$, 2, 3, and 4 in Fig. 5(b) for $V_s=7$ eV and $V_i=0$. Although the finesse of the resonator has increased, we do not find any additional peaks in this case for the voltage range that we have studied. When the interface δ-function strength increases, new structure arises between the $m=2$ and 3 standing-wave peaks, and the $m=3$ and 4 standing-wave peaks are displaced to higher biases. This new structure has been labeled $n=1$ in Fig. 5(c), corresponding to the formation of the $n=1$ standing wave shown schematically in Fig. 4. *The peak height depends primarily on the scattering potential strength, whereas the peak position is a sensitive function of the spatial separation between the scattering potentials, varying almost as* $1/Z_0^2$. The result shown in Fig. 5(c) is obtained with $V_s=V_i=7$ eV Å and $Z_0=1.44$ Å. In Fig. 5(d) we show an experimental spec-

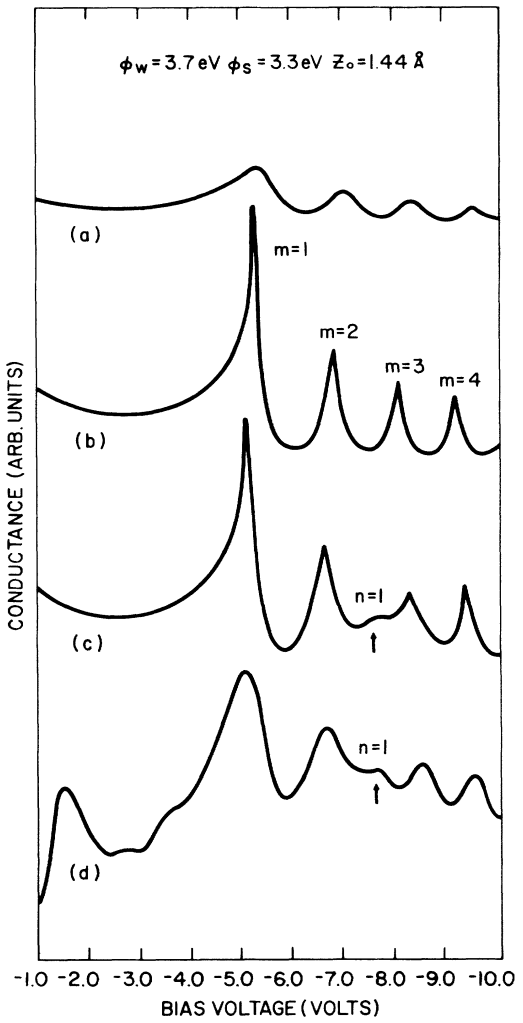

FIG. 5. Calculated conductance vs applied bias spectra for (a) $V_s = V_i = 0$, (b) $V_s = 7$ eV Å, $V_i = 0$, (c) $V_s = V_i = 7$ eV Å, and (d) experimental spectrum.

trum taken over a pristine $\sqrt{3}$ area for comparison. Both the position of the resonance and the shift of the higher-order standing-wave peaks are in agreement with the experimental spectrum; however, the experimental data have a larger phase shift which could arise from additional phase shifts upon reflection that are not taken into account in this first-order theory.

In conclusion, we have investigated electron transport through thin overlayers of tin grown on a silicon substrate, and have observed a resonance in the I-V characteristic that depends on the structural integrity of the film. The resonance occurs for overlayers that are continuous on a length scale of the electron's de Broglie wavelength and is absent at film inhomogeneities. By modeling the resonance as a quantum-size effect associated with the discrete levels of a particle confined within a thin layer, we obtain excellent agreement with the experimental spectra. As this QSE is sensitive to the specularity of the reflections from both the surface and buried interface scattering potentials, the scanning capability of the tunneling microscope provides a new contrast mechanism for imaging of buried interface structure.

We would like to acknowledge helpful discussions with R. S. Becker, L. A. DeLouise, C. B. Duke, and T. E. Orlowski. We would also like to acknowledge L. C. Pizzo for help in preparing this manuscript, and R. S. Becker and B. S. Swartzentruber for sharing their computer codes.

[1]G. Binnig, H. Rohrer, Ch. Gerber, and E. Weibel, Phys. Rev. Lett. **50**, 120 (1983).

[2]W. J. Kaiser and L. D. Bell, Phys. Rev. Lett. **60**, 1406 (1988).

[3]G. Binnig and H. Rohrer, Helv. Phys. Acta **55**, 726 (1982).

[4]R. S. Becker, J. A. Golovchenko, and B. S. Swartzentruber, Phys. Rev. Lett. **55**, 987 (1985).

[5]R. S. Becker, J. A. Golovchenko, D. R. Hamann, and B. S. Swartzentruber, Phys. Rev. Lett. **55**, 2032 (1985).

[6]R. C. Jaklevic, J. Lambe, M. Mikkor, and W. C. Vassell, Phys. Rev. Lett. **26**, 88 (1971).

[7]R. E. Thomas, J. Appl. Phys. **41**, 5330 (1970).

[8]B. T. Jonker, N. C. Bartelt, and R. L. Park, Surf. Sci. **127**, 183 (1983).

[9]P. J. Estrup and J. Morrison, Surf. Sci. **2**, 465 (1964).

[10]T. Ichikawa, Surf. Sci. **140**, 37 (1984).

[11]J. Nogami, Sang-il Park, and C. F. Quate, J. Vac. Sci. Technol. A **7**, 1919 (1989).

[12]N. D. Lang, A. Yacoby, and Y. Imry, Phys. Rev. Lett. **63**, 1499 (1989).

[13]J. A. Kubby, Y. R. Wang, and W. J. Greene (to be published).

[14]J. E. Northrup, Phys. Rev. Lett. **57**, 154 (1986).

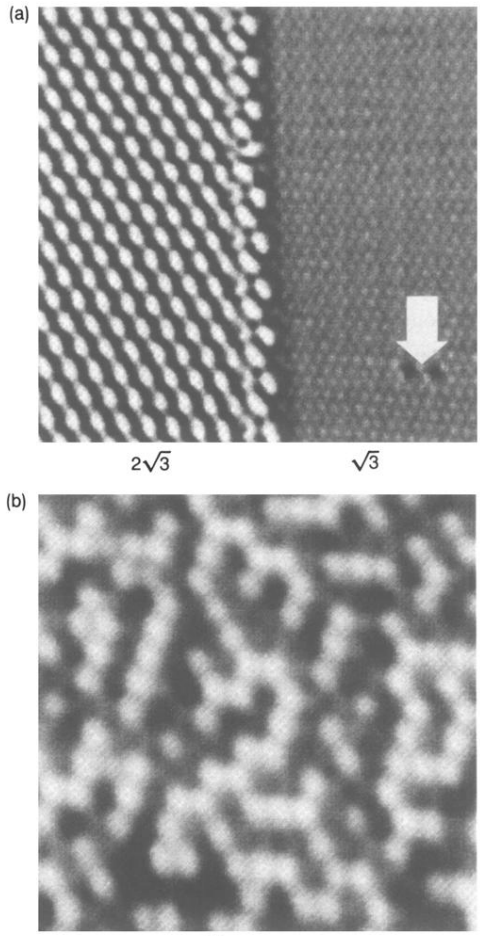

FIG. 1. Tunneling topographs of areas used for standing-wave excitation. (a) 250×250-Å area containing $2\sqrt{3}$ reconstruction on the left and $\sqrt{3}$ reconstruction on the right. The gray scale is keyed to curvature to emphasize local height. (b) 100×100-Å $\sqrt{3}$ mosaic region. The gray scale is keyed to apparent height with a total range of 1.5 Å. Both images were collected with a tip bias of -1.5 V, tunneling from tip to sample at a demanded current of 1 nA.

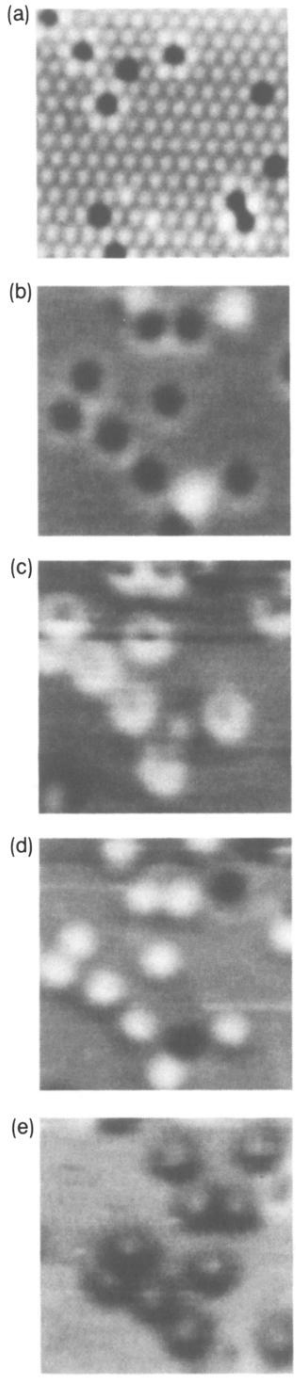

FIG. 3. Conductivity maps of the defective $\sqrt{3}$ area. (a) 100×100-Å topograph at a tip bias of $+1.3$ V and a demanded tunneling current of 1 nA; (b) conductivity map at -7.0 V, (c) at -7.25 V, (d) at -7.50 V, and (e) at -7.75 V.